Electronic Supplementary Material (ESI) for ChemComm.

Ru-coated Metal-organic framework-derived Co-based particles embedded in porous N-doped carbon nanocube as a Catalytic Cathode for Li−O_2 Battery

*Dongdong Li,‡ Haocheng Qi, ‡ Huiming Zhao, Ling Ding, Zhaoxiang Zhang and Ziyang Guo**

Key Laboratory of Eco-chemical Engineering, Taishan scholar advantage and characteristic discipline team of Eco chemical process and technology, College of Chemistry and Molecular Engineering, Qingdao University of Science and Technology, Qingdao 266042, P. R. China
** Corresponding author. Tel & Fax: 0086-21-51630318*
E-mail address: zyguo@qust.edu.cn
‡ Dongdong Li and Haocheng Qi contributed equally to this work.

Experimental Section

Materials

Tetraethylene glycol dimethyl ether (TEGDME, 99.9%) and Li bis(trifluoromethanesulfonyl)imide (LiTFSI, 99.95%) were purchased from Sigma-Aldrich Corporation. Cobalt nitrate hexahydrate ($Co(NO_3)_2$•$6H_2O$, 99 %) were purchased from MACKLIN Reagent Corporation. 2-methylimidazole (99 %) were purchased from J&K Scientific Reagent Corporation. Cetyltrimethy lammonium bromide (CTAB) was purchased from Tianjin BODI Reagent Corporation. $RuCl_3$•xH_2O (35.0~42.0 wt% Ru) was purchased from Aladdin Corporation. All chemicals were used as received without further purification.

Synthesis of ZIF-67 nanocubes. The cubic ZIF-67 was synthesized according to the previous report (ref. S1). In a typical synthesis, 2 mL of aqueous solution containing 58 mg of $Co(NO_3)_2$• $6H_2O$ and 1 mg of cetyltrimethylammonium bromide (CTAB) is rapidly injected into 14 mL of aqueous solution with 908 mg of 2-methylimidazole and vigorously stirred at room temperature for 20 min. Then, the precipitate was collected by repeatedly washing with ethanol for at least 6 times before vacuum drying at room temperature overnight.

The preparation of Co_4N/Co-NC. Firstly, the obtained ZIF-67 was heated to 900 °C under a heating rate of 10 $^oC\ min^{-1}$ with the protection of N_2 gas and further pyrolyzed at the constant temperature of 900 °C for 2 hours. After cooling down to room temperature, the as-prepared Co_4N/Co nanoparticles encapsulated into N-doped porous carbon nanocubes were finally collected. In addition, the as-prepared sample was named as Co_4N/Co-NC.

The preparation of Ru-Co_4N/Co-NC. The obtained Co_4N/Co-NC (160 mg) powder was first added into 200 mL ethylene glycol solution containing 100 mg Ruthenium (Ⅲ) chloride hydrate ($RuCl_3$•XH_2O). [1] After that, the above suspension was treated under the ultrasonication for 1 hour and further refluxed under 170 °C for 3 hours. Then, the Ru-based suspension was centrifuged and the residual solid sample was further washed with deionized water/ethanol for several times. Finally, the resulting

Ru-coated Co_4N/Co-NC (abbreviated as Ru-Co_4N/Co-NC) was dried at 80 °C for 8 hours in the vacuum oven. In addition, characterization instrumentation is given in supporting information.

Synthesis of KB-Ru. KB-Ru was obtained according to the previous report (ref. S4). 50 mg of $RuCl_3$•xH_2O (40% Ru content) was dissolved in 100 mL of ethylene glycol. 80 mg of Super P carbon was added into the solution and was uniformly mixed through an ultrasonic bath. The suspension was refluxed for 3 h at 170 °C. After cooling down, the supernatant was removed and the remnant mixture was centrifuged with deionized water and ethanol several times. The resulting products were dried in a vacuum oven at 80 °C for 12 h. The obtained sample is denoted as KB-Ru.

The preparation of Ru-Co_4N/Co-NC based air cathode. Firstly, Ru-Co_4N/Co-NC, Ketjenblack (KB), and polyvinylidene fluoride binder (PVDF) binder were uniformly mixed by a ratio of 8:1:1 in the N-methyl-2-pyrrolidone (NMP) solution. Then, the obtained slurry was coated on the carbon papers with a diameter of 12 mm to form the air cathodes. Finally, the resulting Ru-Co_4N/Co-NC based electrode were transferred to the vacuum oven and heated at 80 °C for 8 hours to remove NMP solvent. The mass loading of active material in the Ru-Co_4N/Co-NC electrodes is 0.10~0.20 mg cm^{-2}. In addition, the Co_4N/Co-NC, KB and KB-Ru based electrodes were prepared under the same condition.

The fabrication of Li–O_2 batteries with Ru-Co_4N/Co-NC cathodes and the corresponding electrochemical measurements. In the battery fabrication, 1.0 M bis (trifluoromethane) sulfonamide lithium salt (LiTFSI) in tetraethylene glycol dimethyl ether (TEGDME) (1.0 M LiTFSI/TEGDME) was used as electrolyte and the pure metallic Li and the Ru-Co_4N/Co-NC based electrode were applied as anode and cathode, respectively. Firstly, the Li anode, the separator dipping with 1.0 M LiTFSI/TEGDME and the Ru-Co_4N/Co-NC based cathode were orderly assembled in a Swagelok cell. All the above operations were completed in an argon-filled glovebox with the contents of water and oxygen less than 0.1 ppm. There is an O_2 hole with the area of 1.0 cm^{-2} on the cathode side of the Swagelok cell to let O_2 flow in. LAND cycler (Wuhan Land Electronic Co. Ltd) was employed for electrochemical tests. In

addition, the Li–air batteries with Co_4N/Co-NC and KB cathodes were assembled at the same condition. LAND cycler (Wuhan Land Electronic Co. Ltd.) was used for electrochemical investigation.

Detection of the discharge products via XRD or FT-IR technologies. The Li−O_2 battery with Ru-Co_4N/Co-NC cathode was discharged at a current density of 200 mA g^{-1} with a fixed capacity of 4000 mAh g^{-1}. After that, the cell was disassembled in a glove box filled with Ar to obtain the discharged electrode. Then, the discharged electrode was washed with dimethoxyethane (DME) for several times, and then dried under vacuum at room temperature for 6 hours. Next, the discharged electrode was detected by *ex situ* XRD or FT-IR technologies. The Ru-Co_4N/Co-NC electrode before discharge (or after recharge) was detected under the same method.

Characterization instrumentation

XRD measurements were performed on a Bruker D8 Focus power X-ray diffractometer with Cu Kα radiation. Field emission scanning electron microscopy SEM investigations were conducted using a JSM-6390 microscope from JEOL. Transmission electron microscopy (TEM) experiments were conducted using a JEOL 2011 microscope (Japan) operated at 200 kV. The surface of as-prepared sample was characterized by Raman spectroscopy (LABRAM-1B). Specific surface areas were calculated by the Brunaure–Emmert–Teller method. Pore volumes and sizes were estimated from the pore-size distribution curves from the adsorption isotherms using the Barrett–Joyner–Halenda method. X-ray photoelectron spectroscopy (XPS) was conducted with a Thermo Escalab 250 equipped with a hemispherical analyzer and using an aluminum anode as a source. Fourier transform-infrared spectroscopy (FT-IR) tests were performed on a Nicolet 6700 spectrometer. The surface of as-prepared sample was characterized by Raman spectroscopy (LABRAM-1B). LAND cycler (Wuhan Land Electronic Co. Ltd) was employed for electrochemical tests. In situ DEMS was performed using a commercial quadrupole mass spectrometer (Pfeiffer Vacuum, Thermo Star). A quadrupole mass spectrometer (NETZSCH QMS 403 C) with leak inlet was connected to a customized Swagelok cell assembly for DEMS investigation.

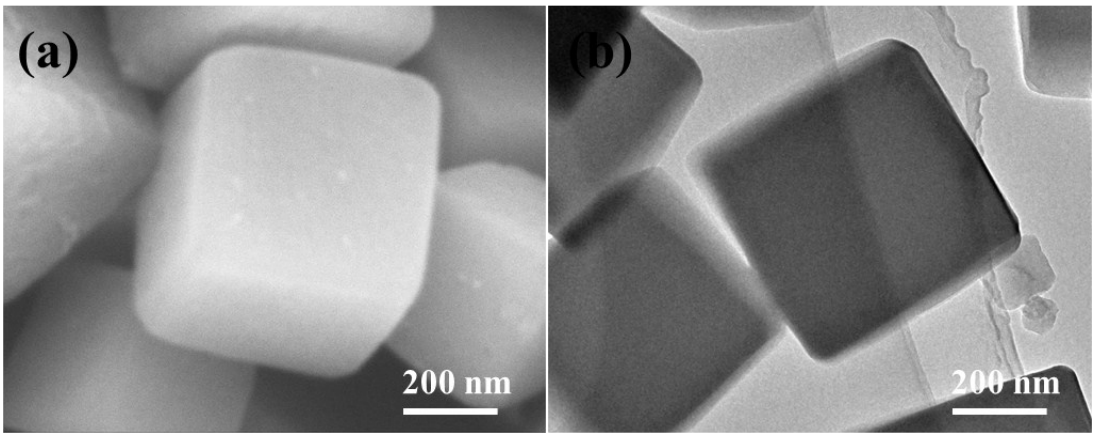

Figure S1 (a) SEM image and (b) TEM image of the cubic ZIF-67.

As shown in **Figure S1**, the as-prepared ZIF-67 are the cubic particles and these particals have very smooth surfaces.

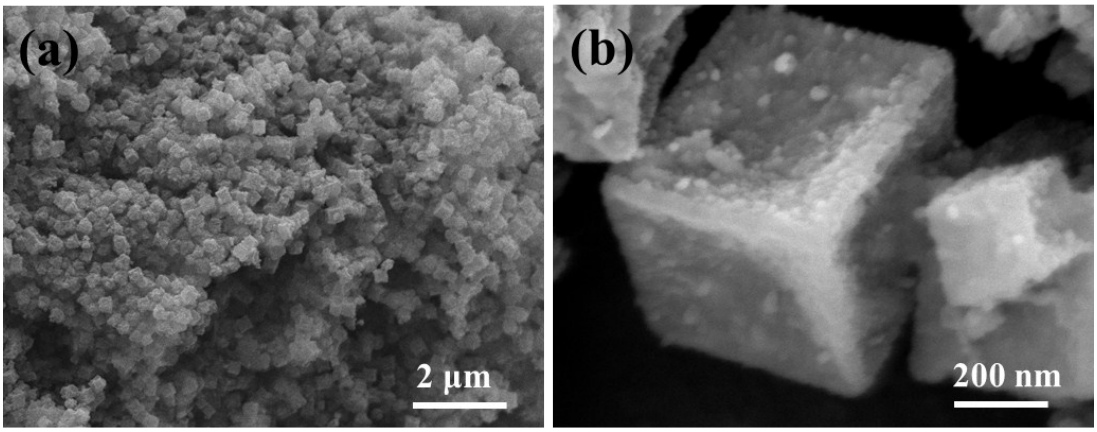

Figure S2 (a-b) the SEM image of as-prepared Co_4N/Co-NC.

As shown in **Figure S2**, the size and polyhedral shape of the ZIF-67 nanoparticles are retained well after thermal treatment, while the surface of the particles becomes much rougher.

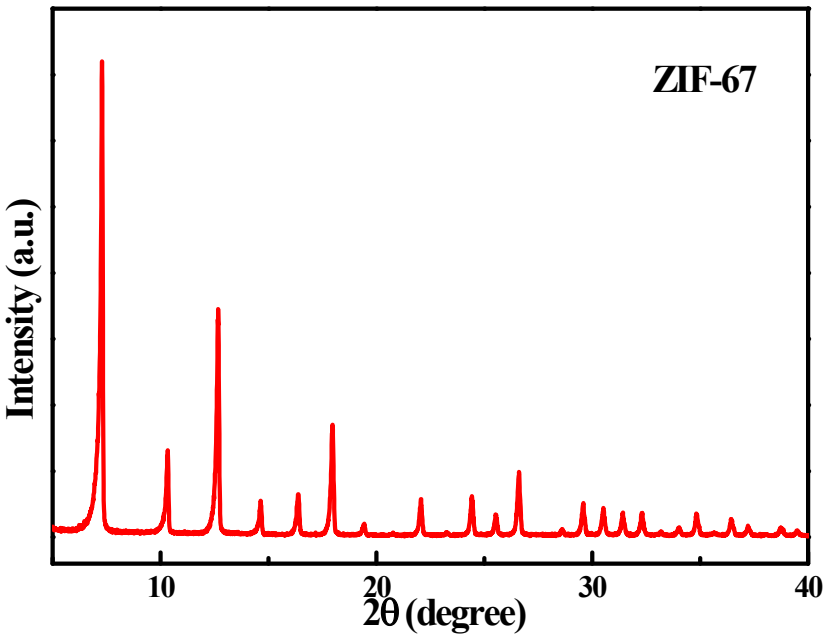

Figure S3 XRD pattern of as-synthesized ZIF-67.

As shown in **Figure S3**, all of the main XRD diffraction peaks are attributed to ZIF-67, which indicats the successful synthesis of ZIF-67. [2]

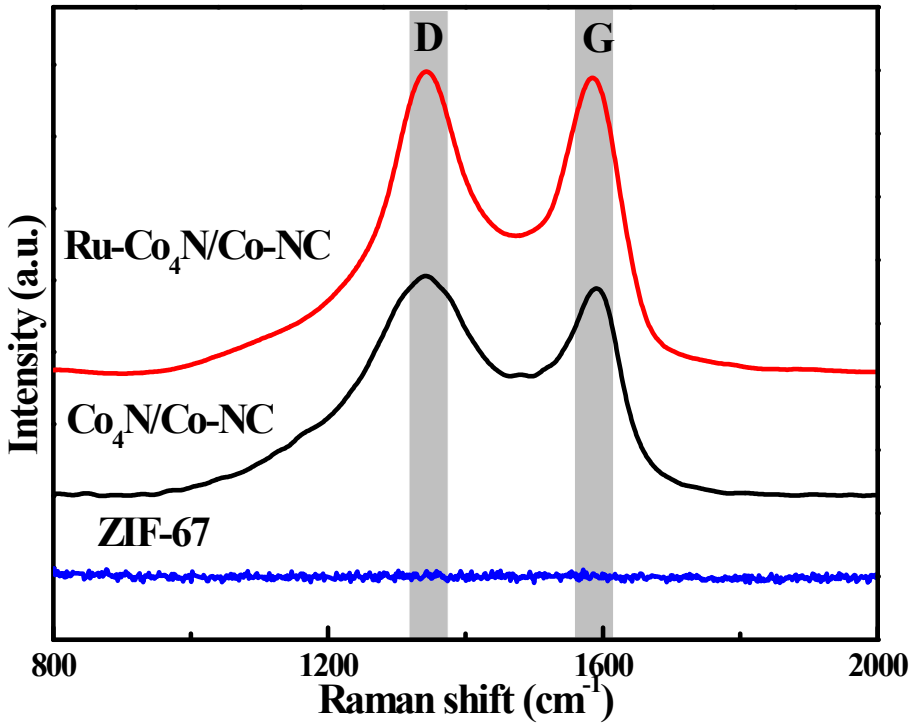

Figure S4 Raman spectra of ZIF-67, Co_4N/Co-NC and Ru-Co_4N/Co-NC in the region of 800-2000 cm^{-1}.

From **Figure S4**, we can see that both the prepared Co_4N/Co-NC and Ru-Co_4N/Co-NC present two typical bands compared with ZF-67 at around 1344 cm^{-1} and 1589 cm^{-1}, corresponded to the D and G bands, respectively. The D and G bands reflect the degree of disorder and graphitization of carbon materials, respectively.

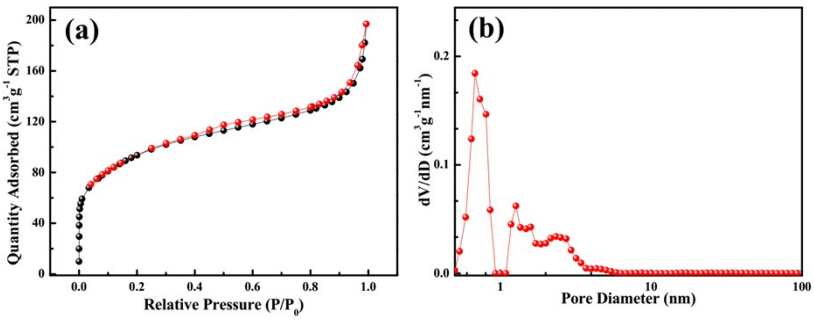

Figure S5 (a) N_2 adsorption/desorption isotherms and (b) pore-size distribution of Co_4N/Co-NC.

As shown in **Figure S5a**, a distinctly increased sorption at low relative pressure (P/P_0<0.05) and a slight hysteresis in a wide relative pressure (P/P_0) range from 0.4-0.8 are observed, suggesting that there are microporous and mesoporous channels in Co_4N/Co-NC. Moreover, it can be detected from **Figure S5b** that there are two main kinds of pores in pore-size distribution curve of Co_4N/Co-NC: micropores (0.5~1.9 nm) and mesopores (2.0~3.5 nm), which is different from that of Ru-Co_4N/Co-NC (**Figure 2f**). This result indicates that the Ru coating layer can regulate the porous nature of Co/Co_4N-NC to some extent.

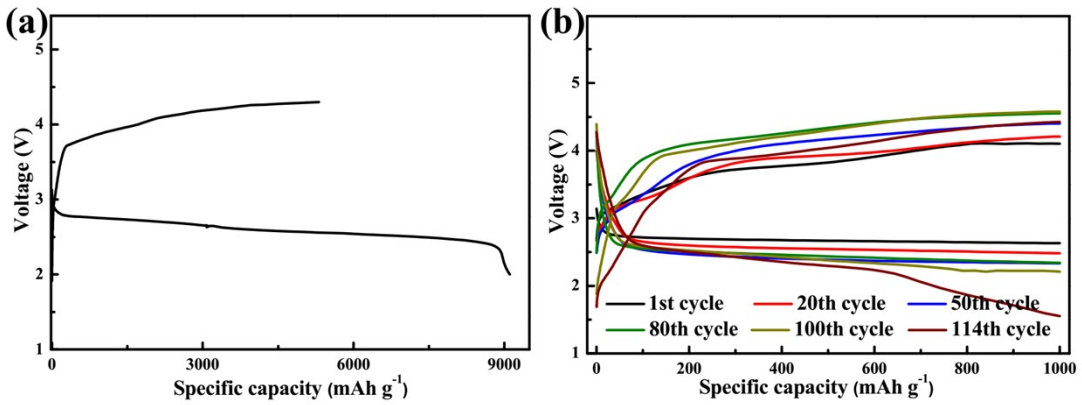

Figure S6 (a) Discharge/charge profiles of the Li–O_2 batteries with KB-Ru electrode at 100 mA g^{-1} between 2.0 and 4.3 V, and (b) Cycle performance of the Li–O_2 batteries with KB-Ru cathode at 500 mA g^{-1} with the fixed capacity of 1000 mAh g^{-1}.

As shown in **Figure S6a**, the discharge capacity of the Ru-KB electrode can reach 9110 mAh g^{-1} at 100 mA g^{-1}, which is lower than that of the Ru-Co_4N/Co-NC cathode. In addition, the cycle performance of the Ru-KB cathode is also studied at 500 mA g^{-1} with a limited capacity of 1000 mAh g^{-1} for comparison (**Figure S6b**). It can be found that the overpotential of Ru-KB electrode at the first cycle is much higher than that of Ru-Co_4N/Co-NC cathode (**Figure S6b** and **Figure 3d**). Moreover, the terminal discharge voltage of the Ru-KB cathode shows an obvious decrease after 114 cycles (**Figure S6b**), while the Ru-Co_4N/Co-NC cathode can be stably operated over 170 cycles (**Figure 3d**). These above results indicate that the electrochemical performances of the Ru-Co_4N/Co-NC cathode are much better than the Ru-KB electrode, which further demonstrates that the unique combination of Ru coating layer and Co-based NC framework can enhance the performance of Li–O_2 batteries.

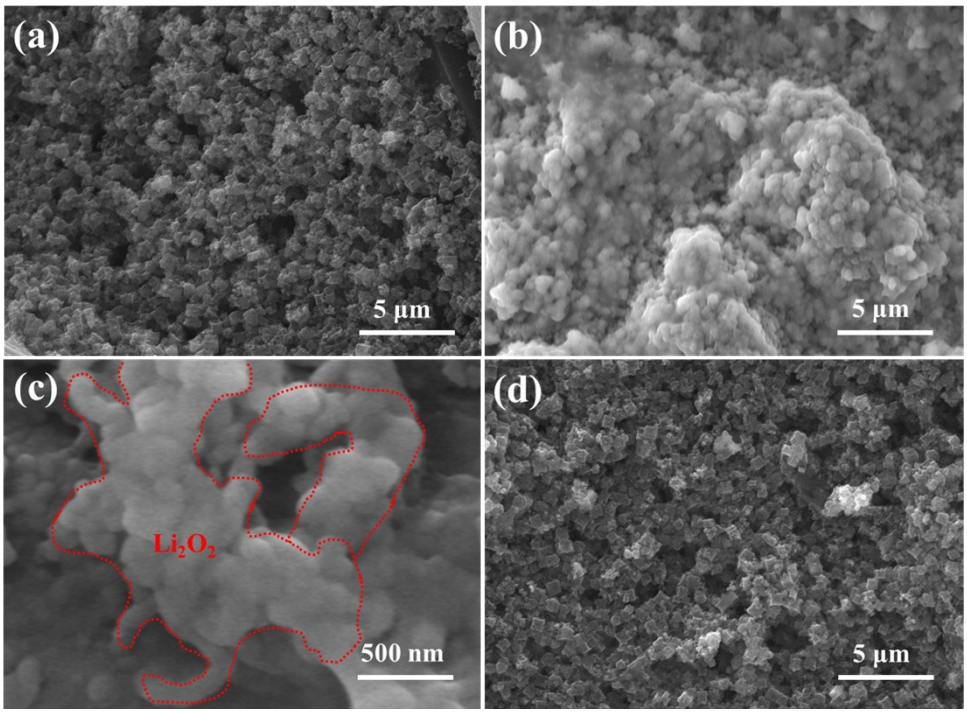

Figure S7 SEM images of (a) before discharged, (b-c) after discharged and (d) after charged Ru-Co_4N/Co-NC electrodes.

As shown in **Figure S7**, there are a number of batteries were dissembled and then characterized using SEM under different conditions for further investigation of the discharge/charge processes of Li−O_2 batteries using Ru-Co_4N/Co-NC catalysts. Compared to the original electrode, the surface of the discharged electrode is fully covered by Li_2O_2 film. However, after the charge process, the discharge products are decomposed and nearly recovered the morphology of the original state.

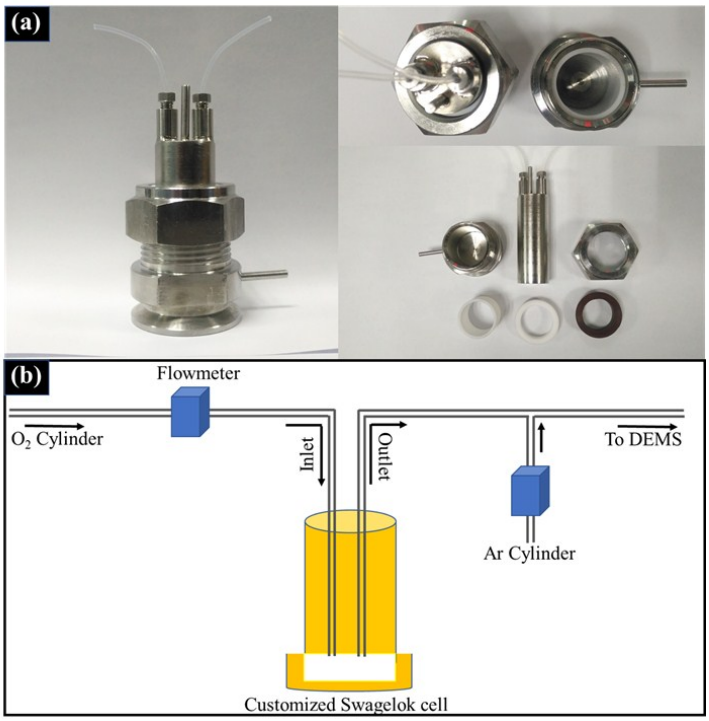

Figure S8 (a) Photo images of the customized Swagelok cell; (b) Schematic illustration of the DEMS analysis system.

The DEMS system was built in-house and guided by the requirement to detect the gases evolved during the charge. A quadrupole mass spectrometer (NETZSCH QMS 403 C) with leak inlet is connected to a customized Swagelok cell assembly (**Figure S8**). The cathode current collector is integrated with two tubes as purge gas inlet and outlet (**Figure S8**). When analyzing the gas consumption over discharge process of Li–air battery, the tested cell should be firstly discharged in the mixed gas of O_2 and Ar. When further analyzing the gas evolution over recharge process of Li–air battery, the system was purged with a pure N_2 stream for 6 hours, and the background for O_2 and CO_2 was calibrated before the charge test and online gas analysis. Purge gas flows were typically 1 mL min^{-1}.

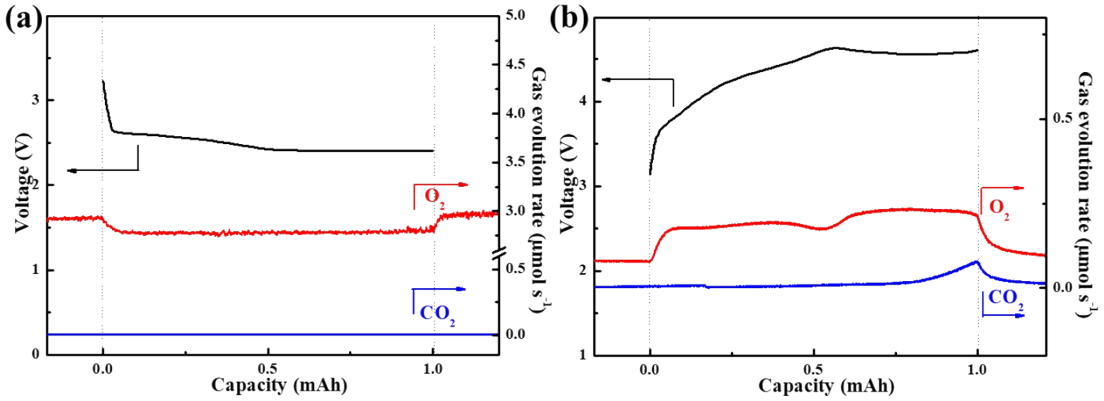

Figure S9 Gas evolution and corresponding discharge-charge curve of Li–O_2 battery using KB cathode at a current of 0.5 mA with a fixed capacity of 1.0 mAh.

The typical galvanostatic discharge profle and the corresponding gas consumption rate of Li–O_2 battery using KB cathode are shown in **Figure S9a**. On discharge O_2 was the only gas consumed and CO_2 were not detected. Unfortunately, lots quantity of evolved CO_2 for KB cathode were showed, which revealed the worry reversibility of KB catalyst in Li–O_2 battery (**Figure S9b**).

Table S1 Summary of cycle performance in various Li–O_2 batteries.

Materials	Cycle performance	Reference
nitrogen-doped $LaNiO_3$	50	Ref.S3
MMC-50	56	Ref.S4
Ru-HOM-AMUW	120	Ref.S5
$CoFe_2O_4$	47	Ref.S6
Co_3O_4@Co_3O_4/Ag	80	Ref.S7
Co[Co,Fe]O_4/NG	110	Ref.S8
CCO@rGO	105	Ref.S9
Co_3O_4/RGO	80	Ref.S10
CNT@Ni@Ni-Co	60	Ref.S11
Co_4N/CNF	100	Ref.S12
CMF-G-Co/CoO	70	Ref.S13
Ru-Co_4N/Co-NC	170	This work

As listed in **Table S1**, the cycling stability of the Li–O_2 battery using Ru-Co_4N/Co-NC cathode in our work is much higher than most of the recent reported Li–O_2 batteries.

References

Ref. S1: S. X. Yang, Y. Qiao, P. He, Y. J. Liu, Z. Cheng, J. J. Zhu, H. S. Zhou, *Energy Environ. Sci.*, 2017, **10**, 972-978.

Ref. S2: Z. Y. Guo, F. M. Wang, Z. J. Li, Y. Yang, A. G. Tamirat, H. C. Qi, J. S. Han, W. Li, L. Wang, S. H. Feng, *J. Mater. Chem. A*, 2018, **6**, 22096-22105.

Ref. S3: J. B. Zhang, C. F. Zhang, W. Li, Q. Guo, H. C. Gao, Y. You, Y. T. Li, Z. M. Cui, K. C. Jiang, H. J. Long, D. W. Zhang, S. Xin, *ACS Appl. Mater. Interfaces*, 2018, **10**, 5543-5550.

Ref. S4: D. Y. Kim, X. Jin, C. H. Lee, D. W. Kim, J. D. Suk, J. K. Shon, J. M. Kim, Y. K. Kang, *Carbon*, 2018, **133**, 118-126.

Ref. S5: W. C. Yang, Z. Y. Qian, C. Y. Du, C. Hua, P. J. Zuo, X. Q. Cheng, Y. L. Ma, G. P. Yin, *Carbon*, 2017, **118**, 139-147.

Ref. S6: J. G. Kim, Y. Noh, Y. M. Kim, S. Lee, W. B. Kim, *Nanoscale*, 2017, **9**, 5119-5128.

Ref. S7: R. Gao, Z. Z. Yang, L. R. Zheng, L. Gu, L. Liu, Y. L, Lee, Z. B. Hu, X. F. Liu, *ACS Catal.*, 2018, **8**, 1955-1963.

Ref. S8: Y. D. Gong, W. Ding, Z. P. Li, R. Su, X. L. Zhang, J. Wang, J. G. Zhou, Z. W. Wang, Y. H. Gao, S. Q. Li, P. F. Guan, Z. D. Wei, C. W. Sun, *ACS Catal.*, 2018, **8**, 4082-4090.

Ref. S9: J. D. Liu, Y. Y. Zhao, X. Li, C. Wang, Y. P. Zeng, G. H. Yue, Q. Chen, *Nano-Micro Lett.*, 2018, **10**:22.

Ref. S10: Z. Zhang, L. W. Su, M. Yang, M. Hu, J. Bao, J. P. Wei, Z. Zhou, *Chem. Commun.*, 2014, **50**, 776-778.

Ref. S11: Z. W. Li, J. Yang, D. A. Agyeman, M. H. Park, W. Tamakloe, Y. Yamauchi, Y. M. Kang, *J. Mater. Chem. A*, 2018, **6**, 10447-10455.

Ref. S12: K. R. Yoon, K. Shin, J. Park, S. H. Cho, C. Kim, J. W. Jung, J. Y. Cheong, H. R. Byon, H. M. Lee, I. D. Kim, *ACS Nano.*, 2018, **12**, 128-139.

Ref. S13: P. Zhang, R. T. Wang, M. He, J. W. Lang, S. Xu, X. B. Yan, *Adv. Funct. Mater.*, 2016, **26**, 1354-1364.